HHS Public Access

Author manuscript

Adv Mater. Author manuscript; available in PMC 2017 October 01.

Published in final edited form as:

Adv Mater. 2016 October ; 28(38): 8524–8530. doi:10.1002/adma.201602373.

Surfactant-stripped Frozen Pheophytin Micelles for Multimodal Gut Imaging

Yumiao Zhang,
Department of Biomedical Engineering, University at Buffalo, The State University of New York, Buffalo, NY, 14260 USA. Department of Chemical and Biological Engineering, University at Buffalo, The State University of New York, Buffalo, NY 14260 USA

Depeng Wang,
Department of Biomedical Engineering, University at Buffalo, The State University of New York, Buffalo, NY, 14260 USA

Shreya Goel,
Materials Science Program, University of Wisconsin-Madison, Madison, WI 53705 USA

Boyang Sun,
Department of Chemical and Biological Engineering, University at Buffalo, The State University of New York, Buffalo, NY 14260 USA

Upendra Chitgupi,
Department of Biomedical Engineering, University at Buffalo, The State University of New York, Buffalo, NY, 14260 USA

Jumin Geng, **Haiyan Sun**,
Department of Radiology, University of Wisconsin-Madison, Madison, WI 53705 USA

Todd E. Barnhart,
Department of Medical Physics, University of Wisconsin-Madison, Madison, WI 53705 USA

Prof. Weibo Cai,
Department of Radiology, University of Wisconsin-Madison, Madison, WI 53705 USA. Department of Medical Physics, University of Wisconsin-Madison, Madison, WI 53705 USA

Prof. Jun Xia, and
Department of Biomedical Engineering, University at Buffalo, The State University of New York, Buffalo, NY, 14260 USA

Prof. Jonathan F. Lovell
Department of Biomedical Engineering, University at Buffalo, The State University of New York, Buffalo, NY, 14260 USA. Department of Chemical and Biological Engineering, University at Buffalo, The State University of New York, Buffalo, NY 14260 USA

Jonathan F. Lovell: jflovell@buffalo.edu

Abstract

Correspondence to: Jonathan F. Lovell, jflovell@buffalo.edu.

A gut imaging contrast agent would benefit from the following: 1) being edible and generally regarded as safe; 2) transiting stably through the intestine; and 3) activity in multiple modalities. We found that Chlorophyll-*a* (Chl), a plant pigment that is ubiquitous in human diets, was amenable to formulation in surfactant-stripped induced frozen micelles (ss-InFroMs). However, Chl ss-InFroM stability was limited in gastric conditions in vitro and in vivo. By demetallating Chl to generate pheophytin-*a* (Pheo), more stable ss-InFroms were obtained which exhibited complete fecal excretion following oral gavage without systemic absorption. Because ss-InFroms could be concentrated to high concentration during the low-temperature stripping of the loose Pluronic surfactant, Pheo ss-InFroMs were used for non-invasive photoacoustic computed tomography of the gut of mice. Unexpectedly, Pheo (but not Chl) ss-InFroms exhibited strong near infrared fluorescence, further enabling non-invasive fluorescence gut imaging. Since Pheo (but not Chl) could be chelated with exogenous metals, Pheo ss-InFroMs could be seamlessly post-labeled with ^{64}Cu for whole body positron emission tomography. Taken together, these results underscore the potential for Pheo, as an edible material, to be re-formulated for higher-order multimodal gut imaging.

Keywords

pheophytin; chlorophyll; multimodal imaging; frozen micelles; gut imaging

Multimodal imaging is being advanced clinically and pre-clinically to provide improved biomedical diagnosis with combined and complementary information.[1,2] A wide range of hybrid imaging modalities have been investigated including positron emission tomography (PET) based multimodalities (e.g. PET/magnetic resonance imaging (MRI),[3] PET/fluorescence imaging (FL),[4] PET/MRI/photoacoustic computed tomography (PACT),[5,6] MRI based multimodalities (e.g. MRI/CT/upconversion (UC),[7] MRI/FL[8]) and CT fused modalities (e.g. CT/MRI/FL,[9] CT/PET/single photon emission computed tomography (SPECT)[10], CT/PET[11,12]) as well as combinations with phototherapies for imaging guided treatments.[13,14] Concurrently, numerous nanoparticles as contrast agents have been designed for use with improved properties in various imaging modalities. Some examples include super-paramagnetic iron oxide nanoparticles, gold nanoparticles,[15–17] polymeric nanoparticles,[18–22] liposomes,[23–25] and up-conversion nanoparticles[26–29]. However, multimodal imaging has not been frequently explored for imaging of the intestine, possibly due to the harsh chemical conditions of the gut. Ideal intestinal imaging contrast agents should be noninvasive and nonionizing, stable in the gastrointestinal (GI) tract and not be absorbed systemically. CT, MRI or ultrasound (US) based modalities for intestinal imaging are, however, limited by drawbacks such as radiation exposure, cost, safety concerns or lack of suitable contrast.

Recently, we developed a surfactant-stripping strategy using hydrophobic naphthalocyanine (Nc) dyes, generating surfactant-stripped induced frozen micelles (ss-InFroMs).[30–32] The process makes use of Pluronic surfactant, which is converted to unimeric form at low temperatures, and is then selectively stripped away with low temperature membrane processing, leaving behind ss-InFroMs with extremely high optical absorption in the near infrared (NIR). This approach provided contrast for functional photoacoustic computed

tomography (PACT) of intestine.[30] PET for whole body intestinal imaging was also possible by simple incubation with the ^{64}Cu ($t_{1/2}$=12.7 h) radioisotope which chelates in the center of Nc macrocycle and the Nc ss-InFroMs are thereby an intrinsic chelator.

Although gut imaging using Ncs is promising, there are potential limitations. For example, fluorescence imaging of intestine was not possible with this approach due to the self-quenching of the extremely hydrophobic dyes. Optical fluorescence imaging, which offers the advantages of low cost, high speed and good resolution, has been shown to be possible for functional imaging of intestinal peristalsis in mice.[33] More significantly, even though Ncs were found to be nearly completely excreted in feces, safety concerns might arise for administering a dye that is not naturally occurring and has not been extensively tested in humans. Porphyrin-related molecules are naturally occurring and have numerous applications for imaging and therapy.[34,35] Here, we demonstrate that demetallated Chlorophyll-a (Chl); pheophytin-*a* (Pheo), which is already present in human diets, can be used for non-invasive, non-ionizing trimodal intestinal imaging with FL, PA and PET. Chl is found in various green vegetables such as spinach[36] and green beans[37], which contain about 0.125% and 0.0045% total mass of Chl, respectively. In this study, Pheo ss-InFroMs were administered in a small volume to mice at a dose corresponding to 46 g spinach/kg body weight or 1.3 kg green beans/kg weight, respectively.

As shown in Fig. 1a, Chl was converted to Pheo after the de-chelation of magnesium in acidic conditions. The displacement of the metal was accompanied by changes in absorbance, with a blue shift of the Soret band (from 428 nm to 408 nm), a red shift of the longest Q band (from 660 nm to 665 nm) and restoration of two other Q bands (between 500 nm and 550 nm) (Fig. 1b).[38] Mass spectrum analysis showed the product had only one single peak, corresponding to the expected Pheo mass (Supplementary Fig. 1). Following magnesium removal, Pheo migrated further than Chl on thin layer silica gel chromatography (data not shown), showing it has less polarity, which is in agreement with the simulated octanal:water Log P partition values of Chl and Pheo as predicted by the ALOGPS algorithm.[39] This is noteworthy since we previously showed that more hydrophobic dyes generally give rise to more stable induced frozen Pluronic micelles.[30]

Next, Pheo ss-InFroMs were made by low temperature surfactant stripping. Pheo was dissolved in dichloromethane (DCM) and was added to a 10% Pluronic F127 (F127) aqueous stirred solution. As the organic solvent evaporated, hydrophobic dyes were driven into the hydrophobic core of Pluronic micelles. At lower temperature, free or loose Pluronic in micelles without cargos loaded changed to unimeric form, which could be effectively removed by centrifugal filtration methods as illustrated in Fig. 1c. No Pheo was found in filtrates (Fig. 1d), indicative of 100% yield for Pheo in ss-InFroMs. Pheo ss-InFroMs were obtained with diameter of about 55 nm, as shown by negative stained transmission electron microscopy (Fig. 1e), which is in agreement with dynamic light scattering measurement (53.7 nm, with polydispersity index of 0.38). Dye extinction coefficient in acetone and ss-InFroM form were calculated to be 5.28×10^4 $M^{-1} \cdot cm^{-1}$ and 4.36×10^4 $M^{-1} \cdot cm^{-1}$, respectively, suggesting dense arrangement of dye and good solubility in micelles (Supplementary table 1). Even though Pheo itself has a smaller extinction coefficient than that of gold nanorods (which are on the order of 10^8–10^9 $M^{-1} \cdot cm^{-1}$) [40], each ss-InFroM

can load thousands of dyes, leading to large value of absorption cross-section. The molar ratio of Pheo to F127 is 4.97 and based on geometrical estimatios, each ss-InFroM contains about 1.5×10^4 dyes, yielding an optical cross-section of 2.5×10^{-12} m^2 (Supplementary Table 1). X-ray powder diffraction (XRD) analysis of freeze-dried Pheo ss-InFroMs did not show any dye crystallinity, suggesting that Pheo was packed irregularly without forming crystals (Supplementary Figure 2).

By using this temperature sensitive critical micellization concentration (CMC) switching and surfactant-stripping method, Pheo ss-InFroMs could be concentrated without noticeable shifting of absorption peak positions as shown in Fig. 1f via absorbance measurements of a concentrated solution using a 10 μm light path length and a 1000-fold dilution of the same solution using 1 cm light path length. Fluorescence of Pheo and Chl ss-InFroMs was examined. Chl ss-InFroms were non-fluorescent, as expected for a densely packed dye. However, Pheo ss-InFroMs were found to retain a substantial relative fluorescence quantum yield (Fig. 1g and Supplementary Fig. 3). Presumably, the displacement of the central metal changed the interaction between the dye and F127, altering the packing of dyes in the micelles, leading to greater micelle fluorescence of Pheo compared to Chl. This phenomenon is illustrated with fluorescence imaging of ss-InFroms as shown in Fig. 1h. Despite being much brighter than Chl, Pheo fluorescence in ss-InFroMs remained largely quenched relative to the pigment in ethanol, where it would be fully solvated without intermolecular interactions to induce quenching. Further investigations are warranted to better explain this phenomenon.

The suitability of Pheo ss-InFroMs for intestinal imaging was assessed *in vitro* and *in vivo*. First, the stability of contrast agents in GI tract was evaluated using simulated intestinal fluid (SIF). As shown in Fig. 2a, after incubation with SIF at 37 °C for 24 hours, Pheo ss-InFroMs were stable under harsh conditions in SIF without appreciable loss of absorption. Under the same experimental conditions, Chl ss-InFroMs were not as stable as Pheo, exhibiting significant loss of absorption, just like gold nanorod as we previously showed [30]. In vivo tests were conducted on mice orally administered 100 O.D. of the two contrast agents respectively. Pheo was recovered 100 % from feces after 24 hours whereas only 70% of Chl was recovered (Fig. 2b). The improved stability of Pheo ss-InFroMs probably arises from the higher hydrophobicity of Pheo, leading to more stable ss-InFroMs, driven by hydrophobic interactions.

The preliminary safety of Pheo ss-InFroMs for the use as an oral contrast agent was examined in vitro and in vivo. As shown in Supplementary figure 4, no toxicity to Caco-2 cell lines was observed up to calculated absorption of 100 (highest level tested) whereas the methylene blue dye induced toxicity when incubated in cell media with an absorbance of 1. Biodistribution for mice orally administered Pheo ss-InFroMs after 24 hours showed no detectable Pheo in main organs including liver, spleen, kidney, heart, lung, brain and also serum. This was not surprising since almost all the nanoparticles were recoverable from feces (Fig. 2c). Encouraged by these results, we administered orally 100 O.D. each mouse. After 24 hours, GI tract and organs were extracted and histology analysis was carried out. No significant acute inflammatory response was induced by Pheo ss-InFroMs as the intestinal villi and crypts seemed intact and healthy, shown in Fig 2d. Similarly, no

noticeable toxicity was observed in main organs, the same as ones in controls with PBS given (Fig 2e).

We used Pheo ss-InFroMs for bioimaging. As shown in Fig 3a, feces that were collected around 3–4 hours after gavage of 100 O.D. of Pheo ss-InFroMs were highly fluorescent, whereas feces from the control group without gavage of any contrast agent exhibited no fluorescence. Fluorescence distribution in intestine could be clearly observed after gavage of Pheo ss-InFroMs whereas no signal was detected before gavage of the contrast agent or after gavage of Chl ss-InFroMs (Fig 3b). The utility of Pheo ss-InFroMs for PA imaging was then assessed. As shown in Fig 3c, contrast agent distribution in the gut was clearly observed. For functional intestinal imaging, a region of interest (ROI) was selected as indicated in Fig 3c. The PA signal within the ROI fluctuated due to peristaltic intestine movement, representing the inflow (indicated by hollow arrows) or outflow (indicated by solid arrows) of the Pheo ss-InFroMs (Fig 3d). Rate of peristaltic intestinal flow was calculated to be close to 30 contractions per minute (Fig 3e).

Although PA contrast imaging has been reported beyond 10 cm in tissues, it is not yet a viable whole body imaging technique.[41] PET is a clinically established quantitative and highly sensitive imaging modality, without any limitation of tissue penetration depth. The PET isotope ^{64}Cu could be readily and efficiently (~ 90% radiolabeling yield) be chelated by Pheo ss-InFroMs, which are an intrinsic copper chelator. ^{64}Cu radiolabeled Pheo ss-InFroMs showed excellent chelation stability in simulated gastric fluid and simulated intestinal fluid, as determined by the retained radioactivity in those conditions (Supplementary Fig. 5). 100 O.D. of ^{64}Cu radiolabeled Pheo ss-InFroMs (~ 10.2 MBq) was orally administered per mouse. As shown in Fig 3f, after only 30 min, radioactivity was seen in the stomach and upper intestine until 4 hours post gavage. As [^{64}Cu] Pheo ss-InFroMs moved down to the large intestine, the signal became attenuated, leaving trace amounts in the feces after 24 hours. Gamma counting demonstrated that close to 93 % [^{64}Cu] of the administered Pheo ss-InFroMs were recovered in feces, as shown in Fig 3g. The slight difference in biodistribution of ^{64}Cu within the Pheo informs and Pheo itself in unlabeled Pheo ss-InFroMs was likely due to a low level of de-chelation of ^{64}Cu from Pheo. Minimal amount of radioactivity retained in all organs with less than 2.5 % injected dose per gram tissue as shown in Fig 3h. The fluorescence and absorption of [^{64}Cu] Pheo ss-InFroMs were examined. After ^{64}Cu labeling, ss-InFroMs still remained highly fluorescent (Supplementary Fig. 6) and did not induce change in absorption properties (Supplementary Fig. 7). Although copper chelation results in quenching of porphyrin fluorescence[42–44], only a small amount of ^{64}Cu is required for radiolabeling (0.4 nmol was used in these experiments). In addition, based on visible light emitted by radionuclides [^{64}Cu] Pheo ss-InFroM displayed potential for Cerenkov imaging as yet another imaging modality for the intestine, as shown in Supplementary Fig. 8.

In summary, Pheo was generated following simple acidification of Chl to remove the central magnesium. Owing to the increase of hydrophobicity, Pheo ss-InFroMs were more stable in the GI tract compared to Chl ss-InFroMs. These surfactant-stripped micelles safely passed through the GI tract and were excreted in feces without inducing any acute toxicity to intestine and main organs. After the removal of the central metal, fluorescence of Pheo ss-

InFroMs was restored, enabling fluorescence imaging of intestine. These studies show proof of principle for multimodal FL, PA and PET gut imaging using a single nanoparticle containing surfactant-stripped micelles of Pheo, which is naturally consumed in human diets already.

Experimental

Materials

Materials were obtained from Sigma unless noted otherwise.

De-chelation of Chl

50 mg Chl (Juntec, Japan) was dissolved in 100 mL diethyl ether (Fisher, # 153099) then 1 mL 1 M hydrochloride acid (Fisher, # 135078) was added dropwise with stirring for 3 hours. 40 mL distilled water was then added to the diethyl ether solution to extract salts. Extraction was repeated another two times. Subsequently, Pheo containing diethyl ether was subjected to rotary evaporation and the dried materials were dissolved in a small amount DCM. Pheo was recovered after adding methanol with the DCM solution. The precipitate was recovered and put in vacuum overnight to remove residual solvent. ~75% conversion yield was achieved.

Preparation of Pheo ss-InFroMs

10 mg Pheo was dissolved in 50 mL DCM, and then added to a 250 mL 10% (w/v) aqueous solution of Pluronic F127 (Sigma, P2443-1KG) with stirring overnight in the dark. The solution was centrifuged at 4,500 × g for 10 mins and no pellet was observed. For small-scale F127 removal process (Fig 1d), 5 mL of the solution was subject to centrifugal filtration (Fisher # UFC9-100-24) at 4 °C until ~200 μL solution was retained. Water was added back the concentrate and the washing procedure was repeated three times. For large-scale washing, filtration (Sartorius vivaflow, 1501008VS) assembled with peristalsis pump (Masterflex L/S) and tubing (masterflex 6434-16) was used to remove excess Pluronic F127. To reach lower temperature and maximize F127 removal, membranes modules, tubing, and solutions to be washed were immersed in ice. The solution was finally concentrated with centrifugal filtration (Fisher #UCF9-100-24) to required concentration.

Characterization of ss-InFroMs

Absorbance was measured with a Lambda 35 UV/VIS or Lambda XLS spectrophotometer (Perkin Elmer) using cuvettes with 1 cm path length for regular absorbance measurement or 10 μm path-length cuvette for high concentration spectral shifting analysis. XRD was measured on a Rigaku Ultima IV, with scanning speed of 0.5 deg/minute at a 0.03 interval. Calculated absorbance is the calculated actual optical absorbance of concentrated Pheo ss-InFroMs for a 1 cm path lenghth cuvette. For 1 cm path length measurements, calculated absorbance equals the absorbance of the diluted solution times the dilution factor; for 10 μm path length measurements, calculated absorbance is absorbance as measured times 1000 (converted to 1 cm path length). For fluorescence spectra, ~10 μL Chl or Pheo ss-infroms were diluted in 2 ml distilled water or ethanol, absorbance at 420 nm was adjusted to be the same then fluorescence was measured on a fluorometer (Photon Technology International).

420 nm was used as the excitation wavelength. For quantum yield calculation, the integrated area between 650 nm and 800 nm emission was used. Fluorescence images were taken on IVIS Lumina II system. Transmission electron microscopy was performed using a JEM-2010 electron microscope with 1% uranyl acetate staining. Mass spectra were obtained using ThermoFinnigan MAT 95 XL, LR and HR work EI electrospray. Dynamic light scattering measurement was conducted on a Nano ZS 90 Zetasizer (Malvern Instruments). For molar ratio calculations, Pheo ss-InFroMs were freeze dried after absorbance measurement. Then acetone was added to the powder for the determination of the mass of dye by measuring the absorbance. F127 amount was determined by cobalt the thiothyanate assay. Briefly, cobalt thiocyanate was prepared by dissolving 0.3 g cobalt nitrate hexahydrate and 1.2 g ammonium thiocyanate in 3 mL water. Then 100 μL of cobalt thiocyanate, 40 μL F127 solution in the concentration range of 0 – 7.5 wt% (more concentrated F127 solutions were diluted to fit that range), 200 μL ethyl acetate and 80 μL ethanol were combined. The mixture was vortexed and centrifuged at 14000×g for 1 min. The supernatant was removed and the blue pellet was washed using ethyl acetate several (~5) times until the supernatant became colorless. The pellet was then dissolved in 1 mL acetone to measure the absorbance at 623 nm. For washing curve in figure 1d, F127 concentration was quantified as above and dye retentions were calculated by measuring the absorbance of filtrates. To assess the stability of Chl or Pheo ss-InFroMs or ^{64}Cu radiolabelled Pheo ss-InFroMs in simulated intestinal fluid (SIF), ss-InFroMs was dialyzed against 200 mL pancreatin-containing SIF (Ricca, # 7109-32). Concentrated ss-InFroMs were diluted with SIF so that the absorbance was close to 1, then dialyzed at 37 °C. Absorbance (for non-radiolabelled nanoparticles) or radioactivity (for radiolabelled nanoparticles) was measured at different time point as shown in figures.

Cell viability

Human epithelial colorectal adenocarcinoma (Caco-2) cells were maintained in DMEM containing 20% fetal bovine serum and 1% penicillin/streptomycin at 37°C under 5% CO_2. Cells were seeded at a concentration of 1×10^4 cells per well. Cells were allowed to attach in media containing serum for 24 hours. Sample of known concentration were added to the wells and were incubated for 24 hours. Media containing sample was removed and washed twice with PBS gently. Immediately, PBS containing XTT (2,3-Bis(2-Methoxy-4-Nitro-5-Sulfophenyl)-2H-Tetrazolium-5-Carboxanilide) (50ug/mL) and PMS (N-methyl dibenzopyrazine methyl sulfate) at 50 and 60 μg/mL respectively were added to each well. Plate was read 2 hours later at 450nm and 630nm. Cell viability was calculated as ratio of viability of treated sample to untreated sample. XTT assay was performed in triplicates and the data represents mean ± standard deviation.

Animal studies

Animal experiments were performed in accordance with the University at Buffalo or University of Wisconsin - Madison Institutional Animal Care and Use committees. 6–8 weeks female ICR mice (Envigo) were used for all experiments. 100 O.D. of Pheo or Chl ss-InFroMs was gavaged in mice that had been fasted overnight. For fecal imaging, feces were collected ~4 hours after gavage for fluorescence or photoacoustic imaging. Mice in control groups were given no contrast agent. To determine recovery percentage of Pheo in feces,

feces were dissolved in 2 mL chloroform followed by homogenization and centrifugation at 3, 000 × g for 3 minutes and absorbance at 660 nm of supernatants was measured. Biodistribution of non-radiolabelled Pheo ss-InFroMs was quantified using the same protocol. For histological studies, organs or intestines were immersed in 10% neutral buffered formalin (VWR # 16004-114) and fixed over 24 hours. The fixed organs were processed through increasing grades of alcohol, cleared in xylene and infiltrated with paraffin (TBS), they were subsequently embedded, cut and stained with haematoxylin and eosin, Finally, the slides were scanned with single slide scanner (Aperio).

Intestinal imaging

For all three imaging methods (FL, PACT, PET), 100 O.D. of Pheo or Chl ss-InFroM was gavaged in mice that had been fasted overnight. For fluorescence imaging of intestine, images were acquired in an IVIS Lumina II system 3 hours post gavage with the mice anesthetized. Control groups were gavaged Chl ss-InFroMs or nothing. For photoacoustic imaging of intestine, a 672 nm excitation light was provided by an Nd:YAG laser with a 10 ns pulse duration and 10 Hz pulse repetition rate. The output of the laser was routed to the imaging region through a 1.2 cm diameter fiber bundle. The maximum light intensity at the skin surface was around 12 mJ/cm^2, which is below the American National Standards Institute (ANSI) safety limitation of 20 mJ/cm^2. The photoacoustic signal was detected by a 128-element linear transducer array (5 MHz central frequency ATL/Philips L7-4). The received signals were first amplified by 54 dB and then digitized by a 128-channel ultrasound data acquisition system (Vantage, Verasonics) with 20 MHz sampling rate. The raw channel data was reconstructed using the universal back-projection algorithm[45] and the reconstructed image could be displayed in real-time during the experiment. For PET imaging, ^{64}Cu was produced via a $^{64}Ni(p,n)$ ^{64}Cu reaction using an onsite cyclotron (GE PETrace) at the university of Wisconsin-Madison. For radiolabeling, 37 MBq of $^{64}CuCl_2$ was diluted in 300 μL of 0.1 M sodium acetate buffer, (pH of 5.5) and added to 400 O.D. nanonaps. The mixture was incubated at 37 °C for 60 min with constant shaking, followed by the purification by Amicon Ultra-4 centrifugal filter unit (Millipore) using PBS. PET scanning was conducted using an Inveon microPET/microCT rodent model scanner (Siemens Medical Solutions USA, Inc.). ICR mice were fasted overnight and gavaged with 100 O.D. pheophytin ss-InFroMs. Static PET scans were performed at indicated time-points post-injection. All PET images were reconstructed using a Maximum a posteriori (MAP) algorithm, without attenuation or scatter correction, and analyzed with Inveon Research Workplace (IRW) software. 24 h post gavage, all mice were sacrificed and organs and intestines were harvested and wet-weighted. The radioactivity in the tissue was measured by WIZARD^2 gamma counter (PerkinElmer) for radiolabel biodistribution.

Supplementary Material

Refer to Web version on PubMed Central for supplementary material.

Acknowledgments

This work is supported by the National Institutes of Health (DP5OD0178980, 1R01CA169365, P30CA014520).

References

1. Kim J, Piao Y, Hyeon T. Chem Soc Rev. 2009; 38:372. [PubMed: 19169455]
2. Rieffel J, Chitgupi U, Lovell JF. Small. 2015; 11:4445. [PubMed: 26185099]
3. Lee HY, Li Z, Chen K, Hsu AR, Xu C, Xie J, Sun S, Chen X. J Nucl Med. 2008; 49:1371. [PubMed: 18632815]
4. Cai W, Chen K, Li ZB, Gambhir SS, Chen X. J Nucl Med. 2007; 48:1862. [PubMed: 17942800]
5. Lin J, Wang M, Hu H, Yang X, Wen B, Wang Z, Jacobson O, Song J, Zhang G, Niu G, Huang P, Chen X. Adv Mater. 2016 n/a.
6. Fan Q, Cheng K, Hu X, Ma X, Zhang R, Yang M, Lu X, Xing L, Huang W, Gambhir SS, Cheng Z. J Am Chem Soc. 2014; 136:15185. [PubMed: 25292385]
7. Zhu X, Zhou J, Chen M, Shi M, Feng W, Li F. Biomaterials. 2012; 33:4618. [PubMed: 22444645]
8. Kim J, Kim HS, Lee N, Kim T, Kim H, Yu T, Song IC, Moon WK, Hyeon T. Angew Chem Int Ed. 2008; 47:8438.
9. Xue S, Wang Y, Wang M, Zhang L, Du X, Gu H, Zhang C. Int J Nanomedicine. 2014; 9:2527. [PubMed: 24904212]
10. Koba W, Jelicks LA, Fine EJ. Am J Pathol. 2013; 182:319. [PubMed: 23219729]
11. Iagaru AH, Mittra ES, McDougall IR, Quon A, Gambhir SS. Nucl Med Commun. 2008; 29:1046. [PubMed: 18987524]
12. Iagaru A, Mittra E, Dick DW, Gambhir SS. Mol Imaging Biol. 2011; 14:252.
13. Cheng L, Liu J, Gu X, Gong H, Shi X, Liu T, Wang C, Wang X, Liu G, Xing H, Bu W, Sun B, Liu Z. Adv Mater. 2014; 26:1886. [PubMed: 24375758]
14. Qiu J, Xiao Q, Zheng X, Zhang L, Xing H, Ni D, Liu Y, Zhang S, Ren Q, Hua Y, et al. Nano Res. 2015; 8:3580.
15. Cheng K, Kothapalli SR, Liu H, Koh AL, Jokerst JV, Jiang H, Yang M, Li J, Levi J, Wu JC, Gambhir SS, Cheng Z. J Am Chem Soc. 2014; 136:3560. [PubMed: 24495038]
16. Arifin DR, Long CM, Gilad AA, Alric C, Roux S, Tillement O, Link TW, Arepally A, Bulte JWM. Radiology. 2011; 260:790. [PubMed: 21734156]
17. Sun IC, Eun DK, Koo H, Ko CY, Kim HS, Yi DK, Choi K, Kwon IC, Kim K, Ahn CH. Angew Chem Int Ed. 2011; 50:9348.
18. Li Y, Lin T, Luo Y, Liu Q, Xiao W, Guo W, Lac D, Zhang H, Feng C, Wachsmann-Hogiu S, Walton JH, Cherry SR, Rowland DJ, Kukis D, Pan C, Lam KS. Nat Commun. 2014; 5:4712. [PubMed: 25158161]
19. Pu K, Shuhendler AJ, Jokerst JV, Mei J, Gambhir SS, Bao Z, Rao J. Nat Nanotechnol. 2014; 9:233. [PubMed: 24463363]
20. Pu K, Mei J, Jokerst JV, Hong G, Antaris AL, Chattopadhyay N, Shuhendler AJ, Kurosawa T, Zhou Y, Gambhir SS, et al. Adv Mater. 2015; 27:5184. [PubMed: 26247171]
21. Miao Q, Lyu Y, Ding D, Pu K. Adv Mater. 2016; 28:3662. [PubMed: 27000431]
22. Lyu Y, Fang Y, Miao Q, Zhen X, Ding D, Pu K. ACS Nano. 2016
23. Mitchell N, Kalber TL, Cooper MS, Sunassee K, Chalker SL, Shaw KP, Ordidge KL, Badar A, Janes SM, Blower PJ, Lythgoe MF, Hailes HC, Tabor AB. Biomaterials. 2013; 34:1179. [PubMed: 23131536]
24. Strijkers GJ, Kluza E, Tilborg GAFV, van der Schaft DWJ, Griffioen AW, Mulder WJM, Nicolay K. Angiogenesis. 2010; 13:161. [PubMed: 20390447]
25. Rieffel J, Chen F, Kim J, Chen G, Shao W, Shao S, Chitgupi U, Hernandez R, Graves SA, Nickles RJ, et al. Adv Mater. 2015; 27:1785. [PubMed: 25640213]
26. Sun Y, Zhu X, Peng J, Li F. ACS Nano. 2013; 7:11290. [PubMed: 24205939]
27. Shen JW, Yang CX, Dong LX, Sun HR, Gao K, Yan XP. Anal Chem. 2013; 85:12166. [PubMed: 24237132]
28. Wu X, Chen G, Shen J, Li Z, Zhang Y, Han G. Bioconjug Chem. 2015; 26:166. [PubMed: 25254658]
29. Chen G, Qiu H, Fan R, Hao S, Tan S, Yang C, Han G. J Mater Chem. 2012; 22:20190.

30. Zhang Y, Jeon M, Rich LJ, Hong H, Geng J, Zhang Y, Shi S, Barnhart TE, Alexandridis P, Huizinga JD, Seshadri M, Cai W, Kim C, Lovell JF. Nat Nanotechnol. 2014; 9:631. [PubMed: 24997526]
31. Lee C, Kim J, Zhang Y, Jeon M, Liu C, Song L, Lovell JF, Kim C. Biomaterials. 2015; 73:142. [PubMed: 26408999]
32. Zhang Y, Song W, Geng J, Chitgupi U, Unsal H, Federizon J, Rzayev J, Sukumaran DK, Alexandridis P, Lovell JF. Nat Commun. 2016; 7:11649. [PubMed: 27193558]
33. Kwon S, Sevick-Muraca EM. Neurogastroenterol Motil. 2011; 23:881. [PubMed: 21624010]
34. Zhang Y, Lovell JF. Theranostics. 2012; 2:905. [PubMed: 23082102]
35. Huang H, Song W, Rieffel J, Lovell JF. Front Phys. 2015; 3:23.
36. Ferruzzi MG, Blakeslee J. Nutr Res. 2007; 27:1.
37. Martins RC, Almeida MG, Silva CLM. Int J Refrig. 2004; 27:850.
38. Huang X, Nakanishi K, Berova N. Chirality. 2000; 12:237. [PubMed: 10790194]
39. Tetko IV, Tanchuk VY. J Chem Inf Comput Sci. 2002; 42:1136. [PubMed: 12377001]
40. Huang H, Liu X, Hu T, Chu PK. Biosens Bioelectron. 2010; 25:2078. [PubMed: 20197234]
41. Zhou Y, Wang D, Zhang Y, Chitgupi U, Geng J, Wang Y, Zhang Y, Cook TR, Xia J, Lovell JF. Theranostics. 2016; 6:688. [PubMed: 27022416]
42. Huang H, Song W, Chen G, Reynard JM, Ohulchanskyy TY, Prasad PN, Bright FV, Lovell JF. Adv Healthc Mater. 2014; 3:891. [PubMed: 24259519]
43. Shao S, Geng J, Ah Yi H, Gogia S, Neelamegham S, Jacobs A, Lovell JF. Nat Chem. 2015; 7:438. [PubMed: 25901823]
44. Carter KA, Wang S, Geng J, Luo D, Shao S, Lovell JF. Mol Pharm. 2016; 13:420. [PubMed: 26691879]
45. Xu M, Wang LV. Phys Rev E Stat Nonlin Soft Matter Phys. 2005; 71:16706.

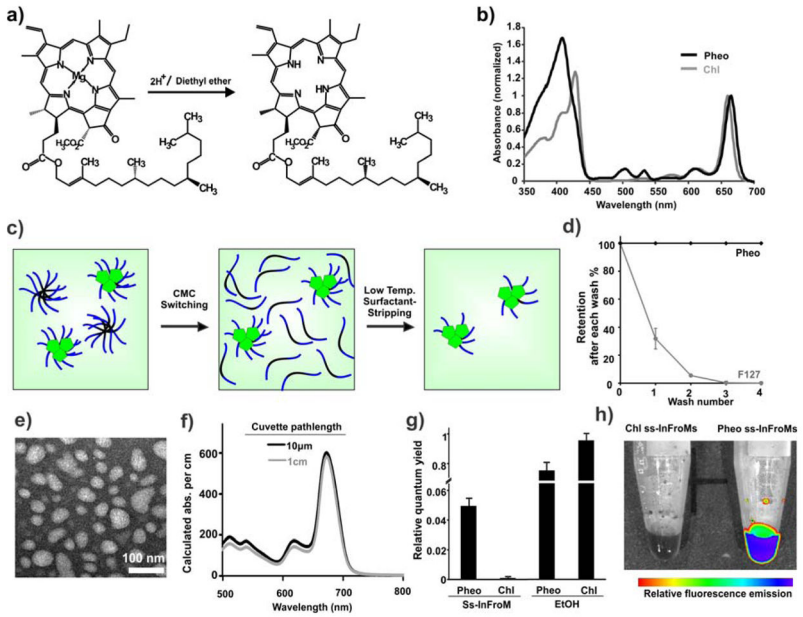

Figure 1. Preparation of Pheo ss-InFroMs

a) Generation of pheophytin-*a* (Pheo) from chlorophyll-*a* (Chl). **b)** Q-band normalized absorbance of Chl and Pheo in chloroform. **c)** Schematic illustration of Pheo ss-InFroM preparation by the critical micelle concentration switching method. Dye, PPO block in F127 and PEO block in F127 presented in green, black and blue color, respectively. **d)** Pheo (black) and F127 (grey) retention as a function of centrifugal filtration washes at 4 °C. n=3. **e)** Negatively stained transmission electron micrograph of Pheo ss-InFroMs. **f)** Calculated absorbance of aqueous Pheo ss-InFroMs obtained by cuvette with light path of 1cm after dilution 1 in 1000 and 10μm cuvette without dilution. **g)** Relative fluorescence quantum yields of Pheo and Chl in ss-InFroM form or in ethanol. **h**) Fluorescence image of Chl and Pheo ss-InFroMs.

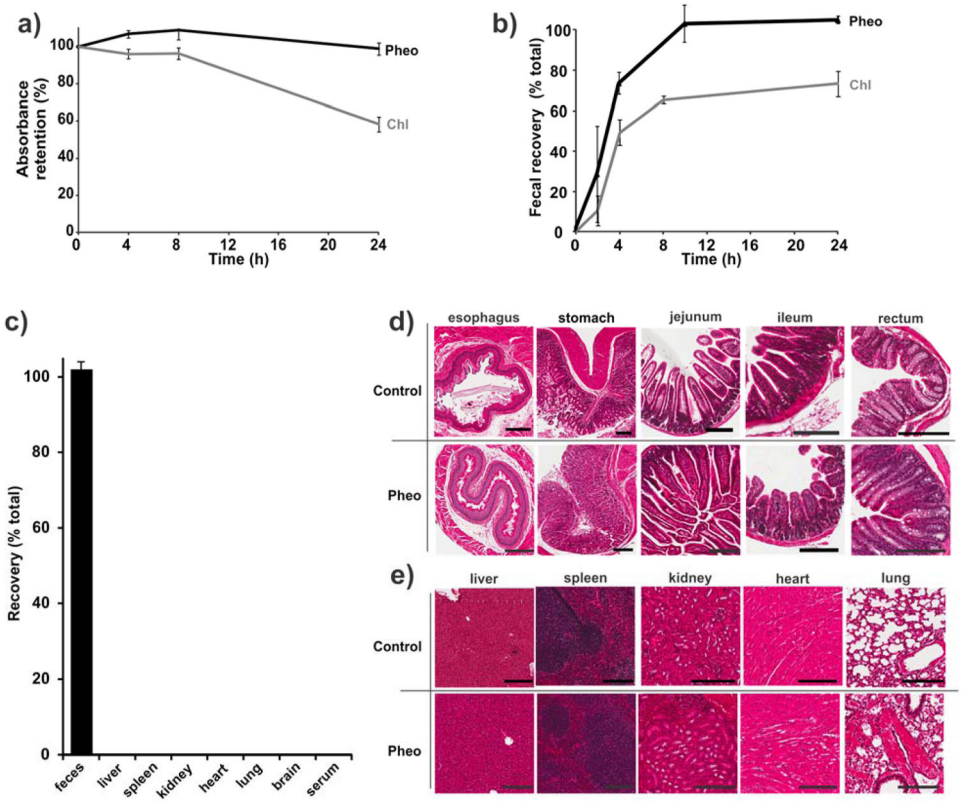

Figure 2. Intestinal stability and gastrointestinal clearance of Pheo ss-InFroMs

a) Retention of Chl and Pheo ss-InFroM absorbance during dialysis in simulated intestinal fluid. **b)** Cumulative recovery in feces within 24 h after gavage of 100 O.D. of Chl or Pheo ss-InFroMs. **c)** Biodistribution of Pheo ss-InFroMs 24 h following gavage of 100 O.D.. Pheo ss-InFroMs were 100% excreted out in feces. No noticeable acute histopathological toxicity was induced by Pheo ss-InFroMs in **d)** GI or **e)** other organs. All scale bars represent 200 μm.

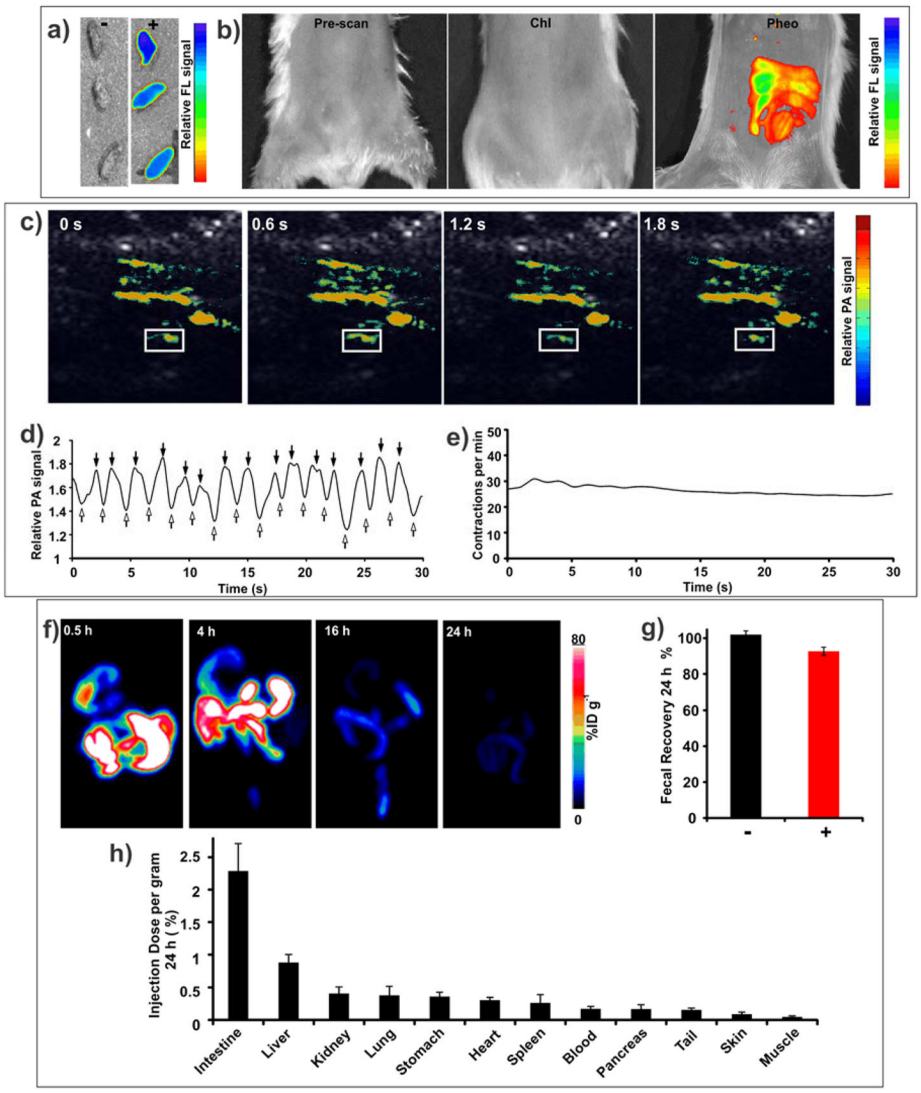

Figure 3. Trimodal imaging of intestine using Pheo ss-InFroMs

a) Fluorescence images of feces with and without administration of 100 O.D. Pheo ss-InFroMs. **b)** Fluorescence images of intestine after gavage of PBS (left), 100 O.D. of Chl ss-InFroMs (middle) or 100 O.D. of Pheo ss-InFroMs (right). **c)** Photoacoustic images of the gut after gavage of 100 O.D. of Pheo ss-InFroMs. Photoacoustic signal is shown in color overlaid on ultrasound gray scale images. **d)** Fluctuation of photoacoustic signal in the region of interest (ROI, indicated by white boxes in Fig. 3c). First derivative zero crossings show the time of maximal photoacoustic contrast inflow and outflow points as indicated by solid and hollow arrows, respectively. **e)** Rate of contractile motion within indicated ROI, plotted over time. **f)** Representative maximum intensity projection PET images of ^{64}Cu Pheo ss-InFroMs at different time points. **g)** Fecal clearance of Pheo ss-InFroMs based on Pheo itself or chelated ^{64}Cu in mice 24 h after gavage of 100 O.D. of contrast agent. **h)** Biodistribution of [^{64}Cu] Pheo ss-InFroMs 24 h after gavage of 100 O.D. Pheo ss-InFroMs.

Most [^{64}Cu] in Pheo ss-InFroMs was cleared in feces. Low amounts ^{64}Cu found in organs were probably caused by a small amount of ^{64}Cu displacement from Pheo.